A Novel Approach for Optimization Control of Dynamic Tracking With Platform Vibration in the Ground Test of Satellite Laser Communication Systems

YUNJIE TENG[1], MIN ZHANG[2], AND SHOUFENG TONG[2]

[1]Institute of Photoelectric Engineering, Changchun University of Science and Technology, Changchun 130022, China
[2]Institute of Space Optoelectronics Technology, Changchun University of Science and Technology, Changchun 130022, China

Corresponding author: Min Zhang (mmiany0815@126.com)

ABSTRACT Vibration interference reduces the precision of the control system and leads to the instability of the satellite optical communication link. So how to improve the tracking accuracy of the terminal system under vibration conditions is an important work for the ground test of satellite laser communication systems. In this paper, the tracking characteristic based on the platform vibration is introduced for coarse tracking and the combination of coarse and fine tracking, we propose a structural decoupling approach and iterative learning control scheme using sliding-mode control to investigate the performance of the tracking system in order to achieve the error minimization, and further to improve the system performance. The scheme is introduced to increase the tracking accuracy and the robustness of the system against external disturbances. The experimental results of the steady-state tracking response and the high tracking precision are carried out on a 4.62 km bidirectional free space laser link experiment, and the obtained test results (less than 2 μrad) demonstrate the effectiveness of the proposed control scheme in suppressing oscillation. This new method is good for the ground test of the satellite laser communication systems.

INDEX TERMS Optical communications, iteration learning control, platform vibration, coarse tracking, fine tracking.

I. INTRODUCTION

Compared with the microwave communication, laser technology offers many potential advantages and has been successfully used in the space communication system, such as the higher data rate and less power consumption [1], [2]. A high precision positioning and tracking of laser beam can provide an efficient media for satellite-to-ground and inter-satellite communication, and its benefits become more notable. Recently, the optical communication has received lots of attention from many countries and has become a hot issue in the field of satellite communication [3]–[5].

Pointing, Acquisition and Tracking (PAT) is a major technology in the laser communication system, which allows for the experimental research of various performance

The associate editor coordinating the review of this manuscript and approving it for publication was Yang Tang.

characteristics [6]. In the process of establishing a laser communication link, the effects of adverse conditions such as the platform vibration can lead to a misalignment between the incoming light and the optical axis of the receiving system [7], [8], thus the investigation of particular laws should be developed for improving the positioning and tracking accuracy of the system.

Dynamic tracking is a formidable engineering problem in the process of laser link establishment, which is further complicated by the platform vibration. The nature of vibration is not fully understood. The jitter of the receiving and transmitting terminals can cause the oscillations of light sensitive elements and light beam, respectively, both of which can lead to a noticeable fluctuation of the spot position on the tracking sensor [9]–[12]. All of these phenomena may result in the interruption of communication. How to realize the design of tracking mode and control algorithm under the vibration

FIGURE 1. An aerial photo of optical propagation path (data from maps.google.com, http://www.google.cn/maps/@30.63).

condition is an important technology for the ground test of satellite laser communication system. In general, the laser beam should be pointed in the field of view of the light sensitive elements, and its deviation from the center of the receiving sensor can be accurately measured. This deviation will provide an error signal to the beam-tracking control system, including the coarse tracking system and the fine steering mirror [13]–[17]. However, successful design for the structural decoupling and compound tracking are capable of reduction for the oscillation caused by beam fluctuation.

Iteration learning control scheme can improve the performance of a system by learning from the previous executions [18]–[20]. To deal with the platform vibration and the lumped disturbances of the system, an ILC scheme with sliding-mode control is developed, this paper presents the adaptive technique for tracking performance improvement, and the control algorithm is implemented in the position tracking loop. The sliding-mode control is employed to suppress the system parameters variation and the external disturbances [21]–[25]. Meanwhile, the iteration learning control is used to inhibit the periodic disturbance. The proposed controller is implemented and the performance of the scheme has been evaluated through experimental investigations. The obtained test results demonstrate the improvements for the steady-state error of coarse and fine tracking, and also validate the effectiveness of the proposed control scheme.

This paper concentrates on an experimental description of a coarse and fine tracking system over a 4.62km near horizontal urban laser link, which verifies the structural decoupling and control scheme under the interference condition. A 4.62km bi-directional free space optical (FSO) communication experiment with a laser propagating through the atmosphere is established to examine the control laws for laser beam tracking, which is described in section II. The new tracking approach that we proposed is introduced in section III, compared with the typical Cassegrain telescope, a decoupling algorithm for the periscope telescope is also conducted in section III. The experimental data is analyzed in section IV.

And the final section summarizes the conclusions for this 4.62km bidirectional free space laser link experiment.

During this experiment, the safety goggles were used to protect the lab members' eyes from being burned by the laser. Moreover, the beams are emitted with a small divergence angle and the directions are adjusted, meanwhile, the optical link is established higher than the buildings near the optical path, so that the laser cannot injure the eyes of the nearby residents, and this experiment is very safe.

II. EXPERIMENTAL SETUP
A. PERISCOPE COMMUNICATION SYSTEM
A 4.62km bidirectional FSO near horizontal laser communication link is established to verify the effectiveness of the novel tracking approach under the fluctuating condition. The experimental system includes two optical communication terminals (CT1 and CT2), with different receiving apertures (70mm and 100mm). A detailed description of this experiment is as follows.

The laser link is built between the two buildings in Wuhan. One of the two communication terminals is located on the 23th floor of a building in Dongxihu area of Wuhan, and the other one is placed on the roof of a building which is beside the Jinyin Lake of Wuhan.

The aerial photo of the laser propagation is shown in Figure 1. The experimental link along the path is complex, which mainly includes a lake, several roads and buildings. The total distance of the optical path is 4.62km, which is measured by GPS.

In this experiment, the two optical communication terminals have similar optical structure. The experimental configuration is shown in Figure 2. Laser is emitted from a laser source, and then reflected onto a separator. The input and output lights have different wavelengths, the input light is transmitted through the separator, while the output light is reflected into a periscope telescope via the separator, and then transmitted outside at the corresponding divergence angle.
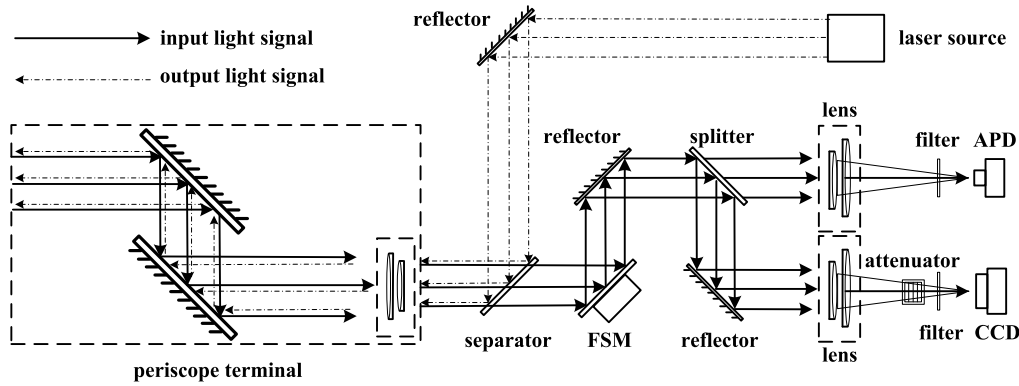
FIGURE 2. Configuration of experimental setup.

The laser is received by the optical communication terminal at the other end of laser link, after propagating through a 4.62km atmosphere turbulent channel.

The input light is received by the periscope telescope. After transmitting through the fast steering mirror (FSM) and the reflector, the laser is separated into two beams of light by a splitter. The two beams will be focused on a complementary metal oxide semiconductor (CMOS) camera and an avalanche photodiode (APD), respectively. One of the two beams which is focused on the APD is used as communication light signal (not mentioned in this paper). Another beam that received by the camera is used as an image miss-distance during tracking process. For the coarse tracking, the CMOS camera is used as full image resolution (1024 × 1024), and the image processing board controls the CMOS camera to record the light spot images at 100 frames/s. For the fine tracking, the CMOS camera is used by reducing the image size to a certain region (160 × 160) by switching windows, and the image processing board controls the CMOS camera to record the light spot images at 2000 frames/s. The parameters of the transmitter and receiver equipment are presented in Table 1.

TABLE 1. Parameters of the experimental systems.

Optical communication system	CT1	CT2
wavelength	780nm	850nm
aperture	70mm	100mm
optical power	300mW	500Mw
focal length	700mm	1000mm
enlargement factor	7	9
CMOS pixels	1024×1024	1024×1024
pixel size	10.6μm	10.6μm

As shown in Figure 2, optical filters are located in front of the communication and detection sensors in order to reduce the interference of the background light.

B. IMPLEMENTATION OF DRIVE SYSTEM
Figure 3 shows the overall scheme configuration of the PMSM servo system for target tracking in this bidirectional communication experiment. The field oriented control (FOC)
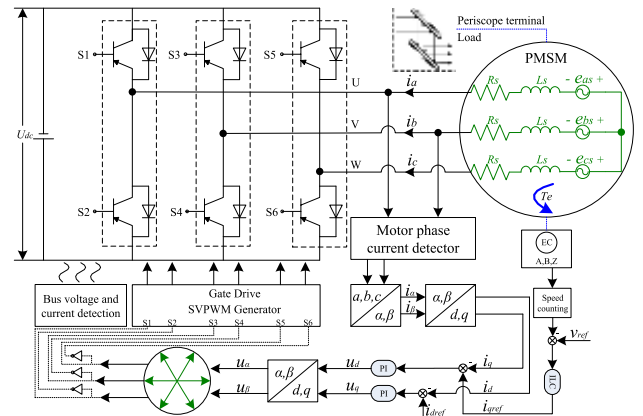

FIGURE 3. Configuration of three-phase PWM control for the PMSM servo system.

method is utilized to perform real-time control of torque drive demand. The q-axis reference current i_{qref} is generated according to the output of the speed controller. PI controllers are used in the inner current loop to provide the control voltages.
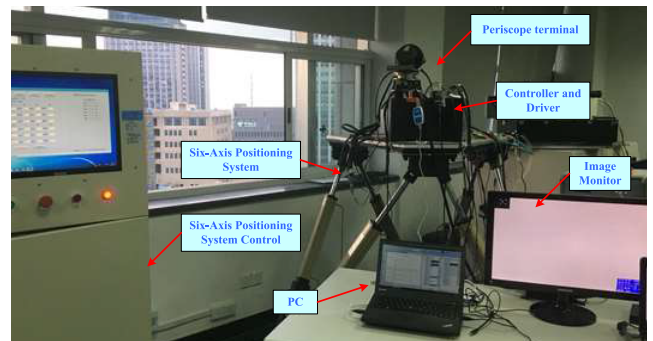

FIGURE 4. Photograph of the communication experimental platform.

A photograph of the experimental platform setup is shown in Figure 4. The current transducer is designed in the drive circuit to test the phase current of the PMSM. It has a high bandwidth output which enables the detection of instantaneous current. The incremental optical encoder is used for the measurement of the position and the speed detection.

The control algorithm is realized using a C program in the ARM-based drive setup using the digital processing chip STM32F407. The parameters of the surface-mounted motor are listed in Table 2.

TABLE 2. PMSM parameters.

Description	Symbol	Value
rated voltage	V	28V
peak current	I_p	3.0Arms
rated current	I_c	1.2Arms
torque constant	K_t	0.7Nm/A
peak torque	T_p	2.1Nm
continuous torque	T_c	0.84Nm
rated speed	n	350rpm

The performance evaluation and comparison of the different tracking target position and acceleration for the disturbance suppression is presented in the following section.

III. ALGORITHMS FOR DYNAMIC TRACKING CALIBRATION

A. STRUCTURAL DECOUPLING METHOD OF PERISCOPE TELESCOPE

Structurally, compared with the typical Cassegrain telescope, the periscope telescope realizes the spatial PAT by rotating the two 45° plane mirrors which are installed on the two orthogonal axis (see Figure 5). This makes the relative position of the plane mirrors and the image acquisition sensor changing constantly (the pink camera as shown in Figure 6).
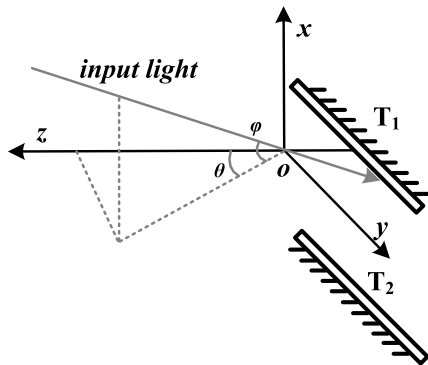

FIGURE 5. Vector of the input light.

However, the image detector provides the actual angular position of the input laser with respect to the center, and this information is used to calculate the correction value of the coarse tracking process. So the structural coupling makes the terminal tracking process complex.

For the image detector, the position information reflects the angle between the vector of input beam and normal line of antenna port. As shown in Figure 5, the coordinate system needs to be explained here, the direction of light emission is defined as the positive *z*-axis, the vector direction of mirror T_2 towards mirror T_1 is the positive *x*-axis. θ and φ are used
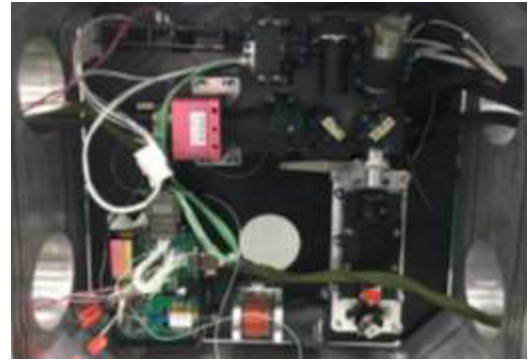

FIGURE 6. Photo of the optical design.

to describe the incident light. The input light can be written as follows:

$$A_{in} = \begin{bmatrix} -\sin\varphi & \cos\varphi\sin\theta & -\cos\varphi\cos\theta \end{bmatrix}^T \quad (1)$$

Beam propagation matrix of the angle measurement system is related to the mirrors T_1, T_2 and the matrix of optical telescope T_{tel}, which is expressed as:

$$T = T_1 \cdot T_2 \cdot T_{tel} \quad (2)$$

According to formula 2, ideally, the vector of incident light obtained from the spot position on the focal plane of CCD can be calculated as:

$$A_{CCD1} = A_{in} \cdot T$$
$$= \begin{bmatrix} 1 \\ -(\sin(\theta_{Az} - \theta_{El}) \cdot \theta - \cos(\theta_{Az} - \theta_{El}) \cdot \varphi) \cdot n \\ (\cos(\theta_{Az} - \theta_{El}) \cdot \theta + \sin(\theta_{Az} - \theta_{El}) \cdot \varphi) \cdot n \end{bmatrix} \quad (3)$$

where θ_{Az} and θ_{El} represent the azimuth and elevation angles, respectively. And n is the enlargement factor of the optical system. The spot position on the focal plane is (Y, Z) relative to the center. Assuming that the camera's front lens has a focal length of f. Then, in the reference coordinate system, the vector of input light is shown as follows:

$$A_{CCD2} = \begin{bmatrix} 1 & Y/f & Z/f \end{bmatrix}^T \quad (4)$$

Considering $A_{CCD1} = A_{CCD2}$, therefore, substituting (3) into (4), we can obtain the angles:

$$\begin{cases} \theta = -\alpha\sin(\theta_{Az} - \theta_{El}) + \beta\cos(\theta_{Az} - \theta_{El}) \\ \varphi = \alpha\cos(\theta_{Az} - \theta_{El}) + \beta\sin(\theta_{Az} - \theta_{El}) \end{cases} \quad (5)$$

where $\alpha = Y/nf$, $\beta = Z/nf$. For the periscope communication terminal, the tracking of the laser is realized by controlling the rotation of the mechanical structure, including the rotation of the azimuth axis and the elevation axis. The rotation matrix around the two axis are described as follows (6) and (7), as shown at the top of the next page, where Ω_{Az} and Ω_{El} are the angles that the experimental terminal needs to rotate. However, the normal line of the emitted light which rotates through the azimuth axis and elevation axis should be

$$S_{Az}(\Omega_{Az}) = \begin{bmatrix} \cos\Omega_{Az} & -\sin\Omega_{Az}\cos\theta_{El} & \sin\Omega_{Az}\sin\theta_{El} \\ \sin\Omega_{Az}\cos\theta_{El} & \cos\Omega_{Az} + 2\sin^2(\Omega_{Az}/2)\sin^2\theta_{El} & 2\sin^2(\Omega_{Az}/2)\sin\theta_{El}\cos\theta_{El} \\ -\sin\Omega_{Az}\sin\theta_{El} & 2\sin^2(\Omega_{Az}/2)\sin\theta_{El}\cos\theta_{El} & \cos\Omega_{Az} + 2\sin^2(\Omega_{Az}/2)\cos^2\theta_{El} \end{bmatrix} \quad (6)$$

$$S_{El}(\Omega_{El}) = \begin{bmatrix} 1 & 0 & 0 \\ 0 & \cos\Omega_{El} & -\sin\Omega_{El} \\ 0 & \sin\Omega_{El} & \cos\Omega_{El} \end{bmatrix} \quad (7)$$

$$\begin{bmatrix} \sin\Omega_{Az}\sin(\theta_{El}+\Omega_{El}) \\ -\sin\Omega_{El}\cos\Omega_{Az}-\sin\Omega_{El}(1-\cos\Omega_{Az})\sin^2\theta_{E1}+(1-\cos\Omega_{Az})\sin\theta_{E1}\cos\theta_{E1}\cos\Omega_{El} \\ -\sin\Omega_{El}(1-\cos\Omega_{Az})\sin\theta_{E1}\cos\theta_{E1}+\cos\Omega_{Az}\cos\Omega_{El}+(1-\cos\Omega_{Az})\cos^2\theta_{E1}\cos\Omega_{El} \end{bmatrix} = \begin{bmatrix} \sin\varphi \\ -\cos\varphi\sin\theta \\ \cos\varphi\cos\theta \end{bmatrix} \quad (8)$$

$$\begin{cases} \Omega_{Az} = \arctan\left[\dfrac{\alpha\cos(\theta_{Az}-\theta_{El})+\beta\sin(\theta_{Az}-\theta_{El})}{\sin\theta_{El}-\alpha\sin(\theta_{Az}-\theta_{El})\cos\theta_{El}+\beta\cos(\theta_{Az}-\theta_{El})\cos\theta_{El}}\right] \\ \Omega_{El} = \dfrac{1-\cos\Omega_{Az}}{\cos\Omega_{Az}}\tan\theta_{El}+\dfrac{-\alpha\sin(\theta_{Az}-\theta_{El})+\beta os(\theta_{Az}-\theta_{El})}{\cos\Omega_{Az}} \end{cases} \quad (10)$$

in the same direction with the system input light, and hence, $A_{in} = S_{Az}(\Omega_{Az})^{-1} \cdot S_{El}(\Omega_{El})^{-1}$, which can be described as follows (8), as shown at the top of this page.

Formula 8 can be simplified as:

$$\begin{cases} \sin\Omega_{Az}\sin(\theta_{El}+\Omega_{El}) = \sin\varphi \\ \cos\Omega_{Az}\sin(\theta_{El}+\Omega_{El}) = \cos\varphi\sin(\theta_{El}+\theta) \end{cases} \quad (9)$$

Substituting (5) into (9) yields the structural decoupling result described as follows:

B. ILC ALGORITHM DESIGN USING SLIDING MODE CONTROL TECHNIQUE

According to modern control theory, we further take the state variables of speed, the parameter variations and the external disturbance into account, the PMSM dynamic system is considered as the following state-space form:

$$\begin{cases} \dot{x}(t) = f(x,t) + bu(t) - r(t) - B(x,t) \\ y(t) = x(t) \end{cases} \quad (11)$$

where the measureable system state $x(t) = \omega$ and $u(t) = i_{qref}$ are the state variable of speed and the control input, respectively, and $y(t) = \omega$ is the system output. Furthermore, b is a known constant, and also it is not zero, $f(x,t)$ represents an unknown state-dependent function that needs to be learned, $r(t)$ represents the system parameter variation and the external disturbances, $B(x,t)$ is the known function of friction torque.

To achieve the control objective, setting ω_{ref} as the desired speed signal, the speed-control algorithm should ensure that the actual running speed tracks the reference speed ω_{ref} accurately under the occurrence of disturbances, where $e(t)$ is the tracking error of the output speed that is defined as $e(t) = \omega_{ref}(t) - \omega(t)$.

Subsequently, the novel control law $u(t)$ is designed for this nonlinear control system (11).

Considering the system (11), the typical sliding-mode surface is defined as follows:

$$s(t) = e(t) + c\int_0^t e(\tau)d\tau \quad (12)$$

Such sliding-mode surface can guarantee asymptotical stable of the sliding-mode, where $c > 0$, satisfying the Hurwitz polynomial, and the asymptotic rate of the convergence is in direct with the value of c.

Then, taking the time derivative of the linear sliding-mode surface. Differentiating both sides of (12) with respect to time t yields

$$\dot{s}(t) = \dot{e}(t) + ce(t) \quad (13)$$

Substituting (11) into (13) yields

$$\dot{s}(t) = ce(t) + \dot{\omega}_{ref}(t) - f(x,t) - bu(t) + r(t) + B(x,t) \quad (14)$$

Formula (14) can be interpreted as sliding-mode surface dynamics. In general, the control input is designed to force the system motion trajectory toward the sliding-mode surface, the sliding-mode reaching condition $s \cdot \dot{s} < 0$ should be satisfied to ensure the motion system stability. The objective of this work is to design a sliding-mode ILC scheme to accomplish the reaching condition within a finite time interval.

The control input $u(t)$ should be designed in such way that the sliding-mode reaching condition is met. Thus, the equal reaching law is chosen as follows:

$$v(t) = \dot{s}(t) = -\beta_1\text{sgn}(s) - \beta_2 s(t) \quad (15)$$

Substituting (15) into (14) yields a sliding-mode ILC controller, the control input $u_k(t)$ at k_{th} iteration can be designed as follows:

$$u_k(t) = b^{-1}(ce_k(t) + \dot{\omega}_{ref}(t) + B(x_k,t) - \hat{f}(x_k,t) - v_k(t)) \quad (16)$$

where k is the number of iteration, and $x_k(t)$ represents the state variable of the system at k_{th} iteration. The estimation of $f(x,t)$ indicates the recursive control part, which can be used for learning the unknown state-dependent function $f(x,t)$, and it can be generated as the following update law:

$$\hat{f}(x_k, t) = \hat{f}(x_{k-1}, t) - q(\eta_1 \mathrm{sgn}(s_k) + \eta_2 s_k(t)) \quad (17)$$

where q, η_1 and η_2 indicate the number of positive constants, and $s_k(t)$ represents the sliding-mode surface dynamics at the k_{th} iteration.

Therefore, substituting the sliding-mode ILC law (16) into (14), the sliding surface dynamics can be simplified as:

$$\dot{s}_k(t) = \left(\hat{f}(x_k, t) - f(x_k, t)\right) + (v_k(t) + r_k(t)) \quad (18)$$

The above equation reveals that, if estimated value can accurately learn from $f(x,t)$, the equal reaching law $v(t)$ can dynamically reduce the effect of the lumped disturbances $r(t)$, then the sliding-mode surface $s(t)$ is convergent.

According to the Lyapunov theorem [26]–[28], the sliding-mode control method needs to satisfy the existing condition of the algorithm and realize the effective suppression of the system interference. However, in practical system application, it is difficult to obtain the accurate value of the lump disturbances. Also the large gain can cause the oscillation phenomenon and excite the high frequency dynamic. In order to overcome these shortcomings, an adaptive approach is employed to estimate the lumped disturbances $r(t)$ online, the estimated value is used for compensation in the control law.

$$u_k(t) = b^{-1}\Big(ce_k(t) + \dot{\omega}_{ref}(t) + B(x_k, t)$$
$$-\hat{f}(x_k, t) - v_k(t) + \hat{r}_k(t)\Big) \quad (19)$$

where $r_k(t)$ represents the estimated lumped disturbances, which is adapted based on the following update law:

$$\hat{r}_k(t) = \gamma s_k(t) \quad (20)$$

where γ is the learning constant of adaptive control law, and $\gamma > 0$. The estimated error is defined as $\tilde{r}_k(t) = \hat{r}_k(t) - r_k(t)$.

Controller (19), together with (15), (17), (20), defines the ILC scheme with adaptive sliding-mode control technology.

Substituting (19) into (14) yields

$$\dot{s}_k(t) = \left(\hat{f}(x_k, t) - f(x_k, t)\right) + v_k(t) - \left(\hat{r}_k(t) - r_k(t)\right) \quad (21)$$

Equation (21) reveals that, if estimated value can accurately learn from $f(x,t)$, the equal reaching law $v(t)$ can dynamically attenuate the error of the estimated lumped disturbances, then the sliding-mode surface $s(t)$ is convergent. The controller structure is given in Figure 7.
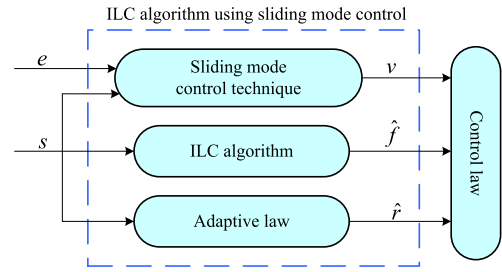

FIGURE 7. Block diagram of the sliding mode ILC controller.

IV. DATA ANALYSIS AND DISCUSSION

The experiment has been carried out from April 2018 to June 2018. In this section, several graphs are presented to illustrate the experimental results, which are derived from the combination of structural decoupling and ILC sliding mode control methods mentioned above. The main objective is to describe the ability of the proposed control algorithm for the suppression of platform vibration and improvement of tracking accuracy of laser beam in the communication link. The PI controller is used for the internal current loop in the two methods, and the parameters are designed all the same: d-axis current controller: $K_{cp} = 3.5$ and $K_{ci} = 0.7$, q-axis current controller: $K_{cp} = 3.5$ and $K_{ci} = 0.7$. The parameters design for the ILC with sliding mode controller: $c = 0.8$, $k = 700$, $\beta_1 = 46$, $\beta_2 = 120$, $q = 0.3$, $\eta_1 = 0.7$, $\eta_2 = 0.4$ and $\gamma = 0.05$. The control frequency for the coarse tracking and the combination of coarse and fine tracking is 100Hz and 2kHz, respectively.

The configuration of the PAT system consists of two tracking modes. One is the dynamic coarse tracking process, in which the image miss-distance on the camera is received as the feedback value in the optical close-loop, then the control value is computed, and the periscope terminal implements the coarse tracking by driving the azimuth axis and elevation axis. The other one is the combination of coarse and fine tracking, the fine tracking mode uses the feedback of the high frame-rate camera based on the coarse tracking described above, the periscope terminal use the FSM position as the feedback value for the following movement, at the same time, this method can solve the problem of the small scope of FSM actuator in the large range tracking process. When the vibration setting and tracking conditions are determined, during the operation, the dynamic response of PAT's position variable is recorded, also including the monitoring of the platform vibration waveform, coarse tracking error, and the errors in coarse and fine tracking.

Data selection was mainly based on the effectiveness of this novel approach and whether the measurement results were available for analysis. Another selection criterion was for different tracking conditions which are based on the 4.62km bi-directional FSO laser link, i.e., different platform oscillation frequency and peak acceleration. Some experimental data are used. As an example, partial data are shown in the following figures. Figures 8-13 present
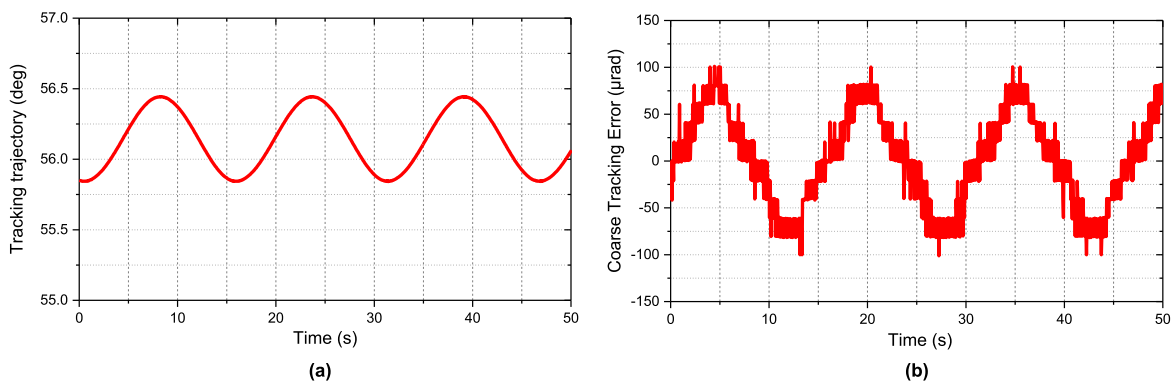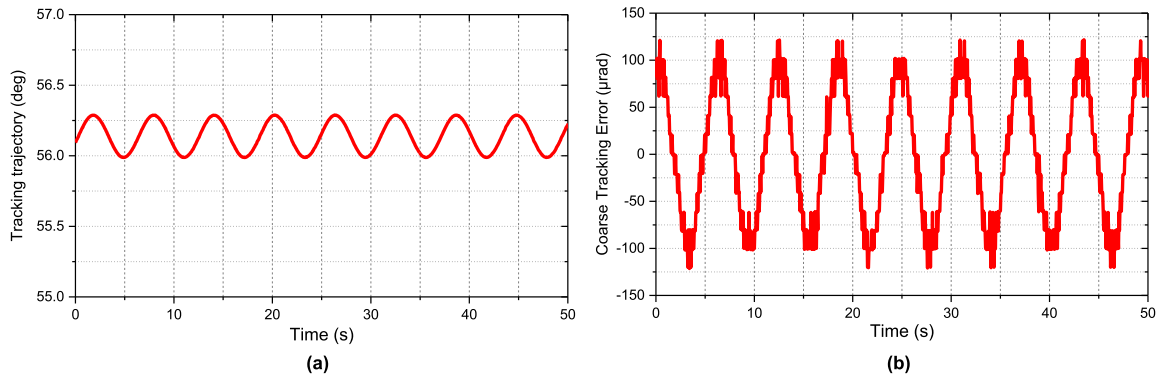
FIGURE 8. Experimental results of coarse tracking, in which the period of platform vibration is 15s and the maximum acceleration is 0.053°/s². (a) Tracking trajectory of periscope telescope. (b) Coarse tracking error.
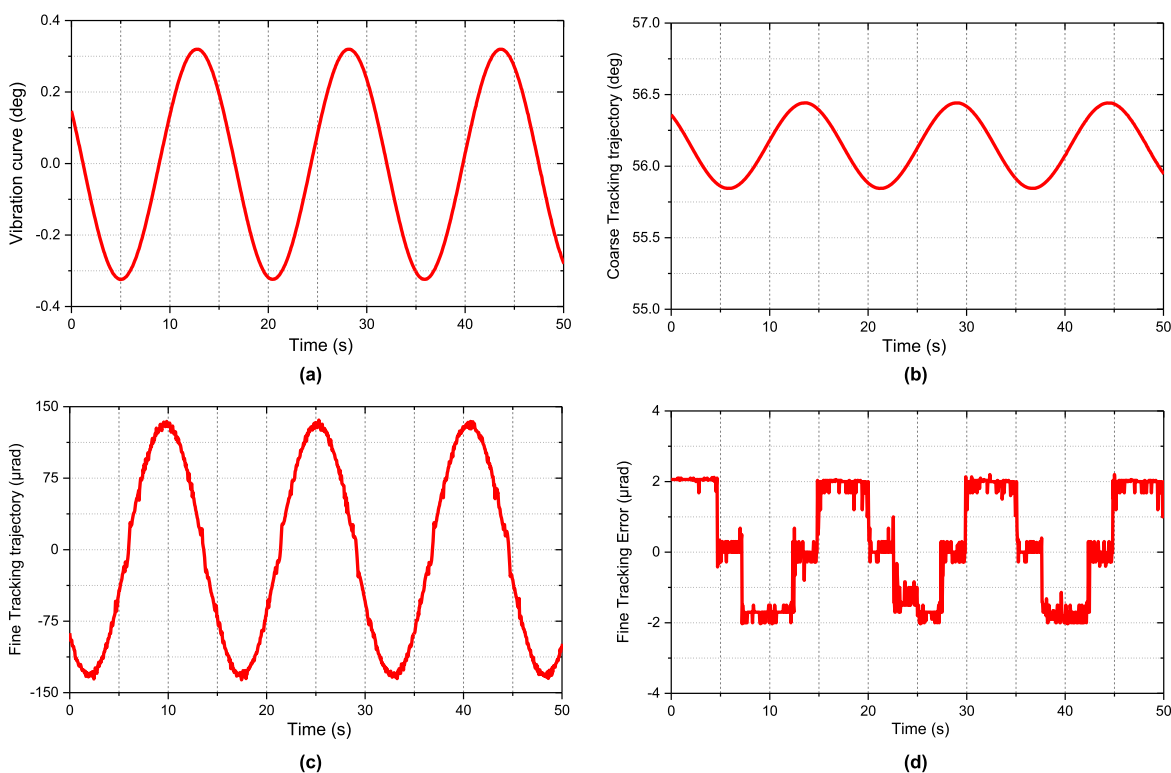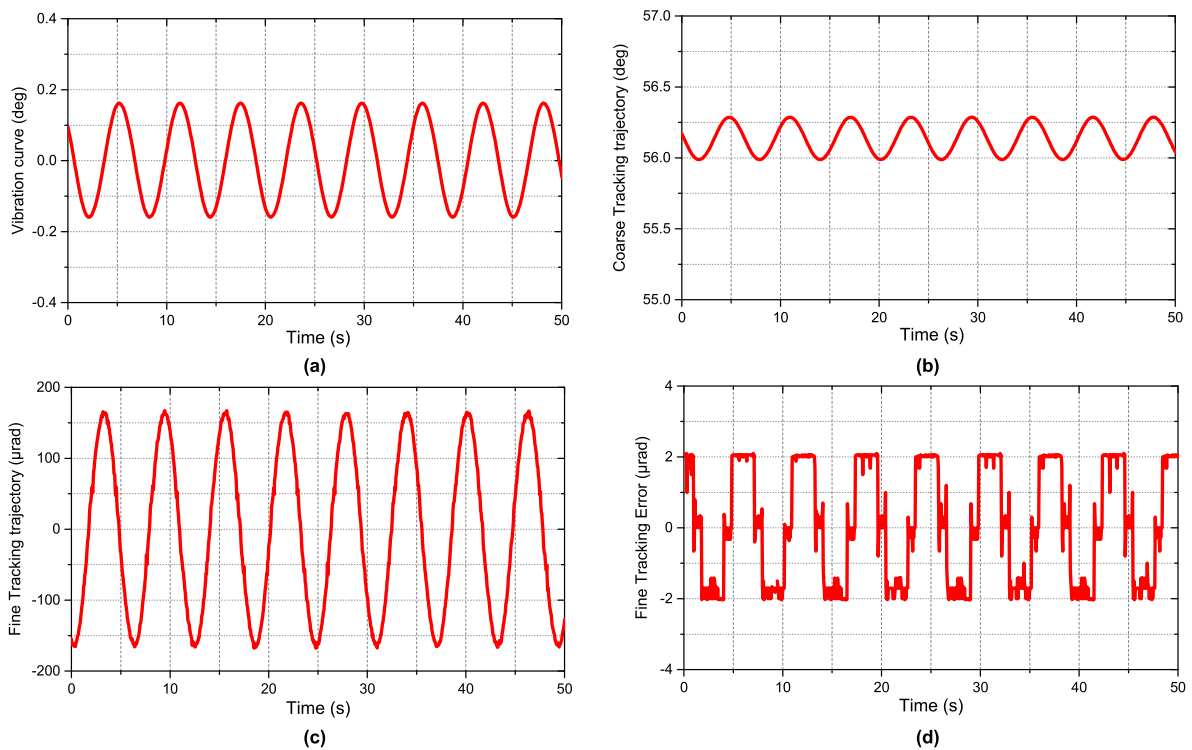

FIGURE 9. Experimental results of the combination of coarse and fine tracking, in which the period of platform vibration is 15s and the maximum acceleration is 0.053°/s². (a) Platform vibration curve. (b) Tracking trajectory of periscope telescope. (c) Tracking trajectory of FSM. (d) Fine tracking error.

data for maximum acceleration of 0.053, 0.164 and 0.109, respectively. Figures. 8, 10, 12 summarize the initial vibration waves and the data of coarse tracking error under different oscillation conditions. Figures 9, 11, 13 consist of data trials based on the combination of coarse and fine tracking, and each graph contains four subplots, including the platform vibration curve and the position following curve for periscope structure (in the top row of each graph), FSM tracking waveform and fine tracking error (on the bottom row of each graph). The data is measured in different vibration amplitudes and accelerations.

This paper focuses on laser tracking accuracy via the proposed control strategy to suppress platform oscillations on the real communication system. The periscope telescopes are the optical terminal device that provide the bi-directional laser link. In contrast, the vibration platform is a constant source of oscillations, which provides dynamic, unpredictable perturbations adversely affecting the PAT operation. Therefore, whether the communication systems, located on the vibration source, are capable of creating a compensation scheme for jitter effects. The structural decoupling technique and ILC method with sliding mode control are applied to the

FIGURE 10. Experimental results of coarse tracking, in which the period of platform vibration is 6s and the maximum acceleration is 0.164°/s^2. (a) Tracking trajectory of periscope telescope. (b) Coarse tracking error.

FIGURE 11. Experimental results of the combination of coarse and fine tracking, in which the period of platform vibration is 6s and the maximum acceleration is 0.164°/s^2. (a) Platform vibration curve. (b) Tracking trajectory of periscope telescope. (c) Tracking trajectory of FSM. (d) Fine tracking error.

compensation of platform vibration. And the test results are presented in Figures 8-13, respectively, which represents the implementation of this control approach for the 3 cases discussed above, indicates that the oscillations can be drastically reduced by the proposed approach. The effectiveness of the selected technique can be explained by the fast tracking response and the extremely high tracking precision.

The relevant data is shown in each subplot. At first, it appears that higher vibration amplitude (0.6°p-p) with the maximum acceleration (0.053°/s^2) result in the coarse tracking error from -100μrad to 100μrad. Comparing the experimental results in Figure 8 with those in Figure 9, it can

be observed that the error values are suppressed to 2μrad in the coarse and fine tracking mode. This high precision tracking system with laser beam that allows for the establishment of a two-way communication links, which may increase the link stability of the optical communication system with the wave propagating in the atmospheric turbulence conditions. The test results confirm the novel approach that the effect of the fluctuation phenomena is taken as an effective vibration suppression in the ground test of PAT system for a satellite optical communication system.

Furthermore, when the conditions are that vibration amplitude is 0.3°p-p, the maximum acceleration is 0.164°/s^2.
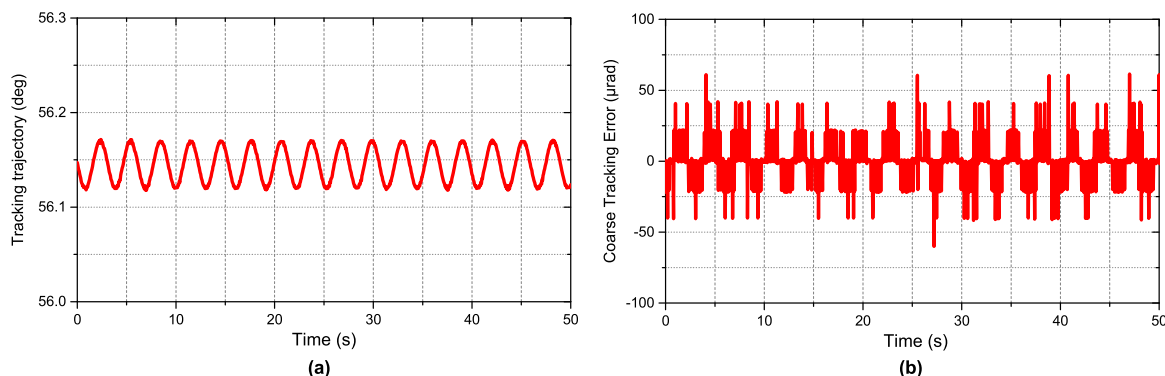
FIGURE 12. Experimental results of coarse tracking, in which the period of platform vibration is 3s and the maximum acceleration is 0.109°/s². (a) Tracking trajectory of periscope telescope. (b) Coarse tracking error.
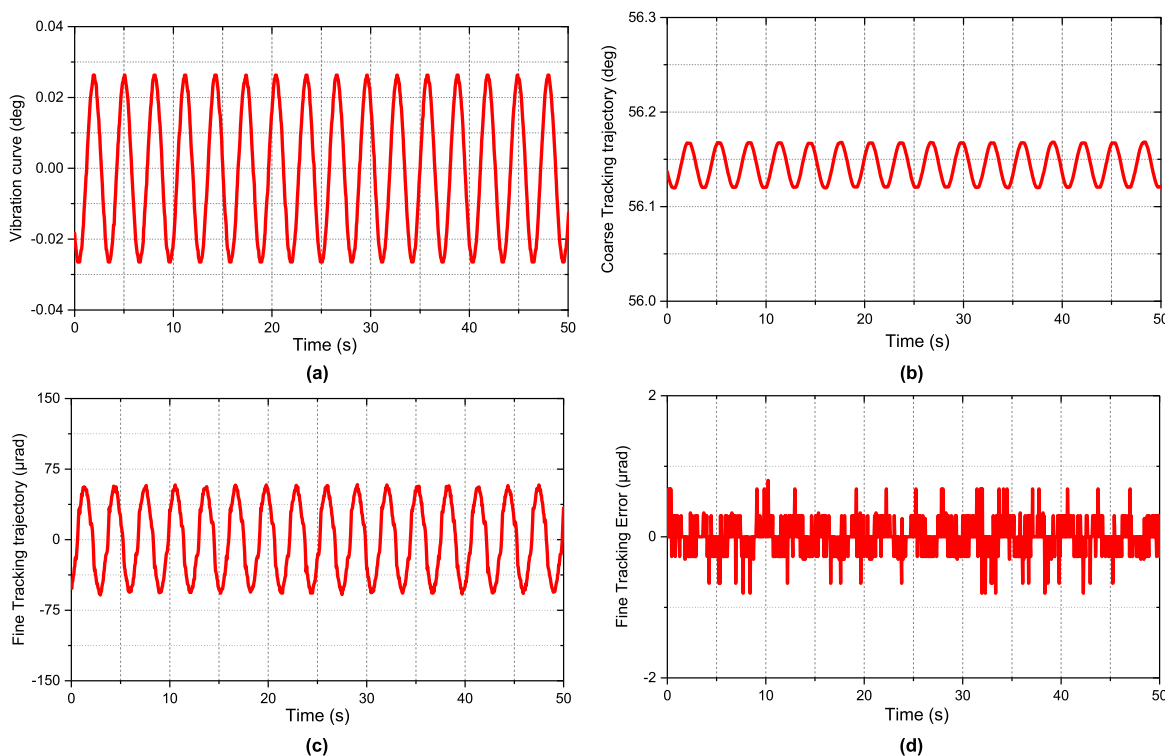
FIGURE 13. Experimental results of the combination of coarse and fine tracking, in which the period of platform vibration is 3s and the maximum acceleration is 0.109°/s². (a) Platform vibration curve. (b) Tracking trajectory of periscope telescope. (c) Tracking trajectory of FSM. (d) Fine tracking error.

For such cases, the comparisons between the coarse tracking and the compound tracking based on the platform vibration of this case are illustrated in Figure 10 and Figure 11, respectively. Due to the increased acceleration, the coarse tracking error changes from -125μrad to 125μrad. However, the successful implementation of the proposed oscillation rejection scheme also can minimize the overall jitter effect on the laser-tracking error. The control law presented in this paper is utilized to suppress vibration characteristics and also improve the system tracking accuracy to 2μrad during coarse and fine tracking operation process, which is consistent with the experimental result (shown in Figure 9(d)).

The corresponding optical link can be maintained stable tracking accuracy under the different oscillation characteristics along the optical path.

Although the dynamic PAT tracking system has been investigated under the two noticeable vibration conditions, it can be expected that the search is carried out in other jitter conditions. Therefore, additional research is necessary to further explore the tracking precision based on the vibration of low amplitude and high frequency. Figures 12-13 are arranged in the same sequence, the oscillation conditions of these figures are that the vibration amplitude is 0.05°p-p, the maximum acceleration is 0.109°/s². In these

TABLE 3. Results of the experiment.

Experiment	Tracking target position (p-p)	Tracking target acceleration	Coarse tracking error (Maximum)	Fine tracking error (Maximum)
first	0.6°	0.053°/s^2	100μrad	2μrad
second	0.3°	0.164°/s^2	125μrad	2μrad
third	0.05°	0.109°/s^2	60μrad	0.8μrad

cases the corresponding coarse tracking error is suppressed from -60μrad to 60μrad. And the error value is suppressed to 0.8μrad in the coarse and fine tracking mode as shown in Figure 13 (d). These experimental results clearly indicate that the proposed control algorithm and tracking approach is capable of the significant of reduction of beam-tracking errors. And the entire communication link system is capable of tracking continuously varying oscillation and acceleration characteristics. The experimental results are listed in Table 3. And then the success and high tracking precision of PAT process in the platform vibration environment on the ground test can guarantee equivalently the establishment and maintenance in the satellite laser communication link with vibration conditions.

V. CONCLUSIONS

A 4.62km bidirectional free space laser link experiment was conducted to investigate the effect of platform vibration. The structural decoupling strategy and iterative learning control using sliding-mode control have been presented for improving the tracking accuracy in this paper. It was found that the tracking data were reasonably tested which consists of three cases collected including different vibration amplitude and acceleration settings. However, it still clearly shows what distinguishes between coarse tracking and the combination of coarse and fine tracking. It was suggested that although the tracking errors of laser beam for the PAT system are not fixed values under different perturbation conditions, but mostly they are less than 2μrad. Additional complicated disturbance cases can be derived in the future works.

In this paper, the tracking characteristic is introduced based on the platform vibration, referring to the new tracking algorithm and its application. Also the comparison of the two tracking forms show that both tracking modes can provide the characteristic of stability for the laser communication link. Especially, it is considered that the combination of coarse and fine tracking based on the novel control strategy is taken as a more effective method for platform vibration in the ground test of PAT system. In addition, the periscope telescope is shown to be a unique experimental terminal for this kind of investigation. The experimental results of the steady-state tracking response and the high tracking precision have been presented to demonstrate the effectiveness in suppressing oscillation of the proposed scheme. This work is also benefit for free space laser communication system design. Future work is progressing, and it is therefore expected that the

algorithm can effectively realize high performance control in much higher acceleration and larger tracking region in the future research.
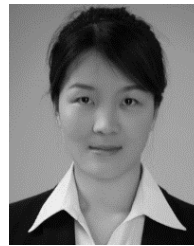
REFERENCES

[1] X. Li, S. Yu, J. Ma, and L. Tan, "Analytical expression and optimization of spatial acquisition for intersatellite optical communications," *Opt. Express*, vol. 19, no. 3, pp. 2381–2390, 2011.

[2] M. Toyoshima, W. R. Leeb, H. Kunimori, and T. Takano, "Comparison of microwave and light wave communication systems in space applications," *Proc. SPIE*, vol. 5296, no. 1, pp. 1–12, Jan. 2005.

[3] R. Lange, B. Smutny, B. Wandernoth, R. Czichy, and D. Giggenbach, "142 km, 5.625 Gbps free-space optical link based on homodyne BPSK modulation," *Proc. SPIE*, vol. 6105, no. 10, Mar. 2006, Art. no. 61050A.

[4] K. Kazaura *et al.*, "Enhancing performance of next generation FSO communication systems using soft computing based predictions," *Opt. Express*, vol. 14, no. 12, pp. 4958–4968, 2006.

[5] W. Du, L. Tan, J. Ma, and Y. Jiang, "Temporal-frequency spectra for optical wave propagating through non-Kolmogorov turbulence," *Opt. Express*, vol. 18, no. 6, pp. 5763–5775, 2010.

[6] V. Utkin, "Discussion aspects of high-order sliding mode control," *IEEE Trans. Autom. Control*, vol. 61, no. 3, pp. 829–833, Mar. 2016.

[7] J. Wang, J. Lv, G. Zhao, and G. Wang, "Free-space laser communication system with rapid acquisition based on astronomical telescopes," *Opt. Express*, vol. 23, pp. 20655–20667, Oct. 2015.

[8] A. Carrasco-Casado, M. Vilera, R. Vergaz, and J. F. Cabrero, "Feasibility of utilizing Cherenkov telescope array gamma-ray telescopes as free-space optical communication ground stations," *Appl. Opt.*, vol. 52, no. 11, pp. 2353–2362, 2013.

[9] M. Toyoshima and K. Araki, "In-orbit measurements of short term attitude and vibrational environment on the engineering test satellite VI using laser communication equipment," *Opt. Eng.*, vol. 40, pp. 827–832, May 2001.

[10] M. J. Curley *et al.*, "Statistical analysis of cloud-cover mitigation of optical turbulence in the boundary layer," *Opt. Express*, vol. 14, pp. 8929–8946, Oct. 2006.

[11] R. H. Vollmerhausen, E. L. Jacobs, and R. G. Driggers, "New metric for predicting target acquisition performance," *Opt. Eng.*, vol. 43, no. 11, pp. 2806–2818, Nov. 2004.

[12] D. H. Tofsted, "Turbulence simulation: Outer scale effects on the refractive index spectrum," United States Army Res. Lab., Adelphi, MD, USA, Tech. Rep. ARL-TR-548, 2000.

[13] Q. Wang, Y. Liu, J. Ma, L. Tan, S. Yu, and C. Li, "Quick acquisition and recognition method for the beacon in deep space optical communications," *Appl. Opt.*, vol. 55, no. 34, pp. 9738–9743, 2016.

[14] I. S. Ansari, F. Yilmaz, and M.-S. Alouini, "Impact of pointing errors on the performance of mixed RF/FSO dual-hop transmission systems," *IEEE Wireless Commun. Lett.*, vol. 2, no. 3, pp. 351–354, Jun. 2013.

[15] A. J. Hashmi, A. A. Eftekhar, A. Adibi, and F. Amoozegar, "Analysis of telescope array receivers for deep-space inter-planetary optical communication link between Earth and Mars," *J. Opt. Commun.*, vol. 283, pp. 2032–2042, May 2010.

[16] E. Lee, J. Park, D. Han, and G. Yoon, "Performance analysis of the asymmetric dual-hop relay transmission with mixed RF/FSO links," *IEEE Photon. Technol. Lett.*, vol. 23, no. 21, pp. 1642–1644, Nov. 1, 2011.

[17] D. M. Freemon, K.-T. Lim, J. Becla, G. P. Dubois-Felsman, and J. Kantor, "Data management cyberinfrastructure for the large synoptic survey telescope," *Proc. SPIE*, vol. 8451, no. 5, Sep. 2012, Art. no. 84510V.

[18] W. Qian, S. K. Panda, and J. X. Xu, "Speed ripple minimization in PM synchronous motor using iterative learning control," *IEEE Trans. Energy Convers.*, vol. 20, no. 1, pp. 53–61, Mar. 2005.

[19] S. Tayebi-Haghighi, F. Piltan, and J.-M. Kim, "Robust composite high-order super-twisting sliding mode control of robot manipulators," *Robotics*, vol. 7, pp. 1–18, Mar. 2018.

[20] K. Jezernik, J. Korelič, and R. Horvat, "PMSM sliding mode FPGA-based control for torque ripple reduction," *IEEE Trans. Power Electron.*, vol. 28, no. 7, pp. 3549–3556, Jul. 2013.

[21] J. Fei and T. Wang, "Adaptive fuzzy-neural-network based on RBFNN control for active power filter," *Int. J. Mach. Learn. Cybern.*, vol. 6, pp. 1–12, Feb. 2018.

[22] Y. Fang, J. Fei, and T. Hu, "Adaptive backstepping fuzzy sliding mode vibration control of flexible structure," *J. Low Freq. Noise Vib. Act. Control*, vol. 37, no. 4, pp. 1079–1096, 2018.

[23] J. Fei and C. Lu, "Adaptive fractional order sliding mode controller with neural estimator," *J. Franklin Inst.*, vol. 355, no. 5, pp. 2369–2391, 2018.

[24] Y. Chu, J. Fei, and S. Hou, "Dynamic global PID sliding control using neural compensator for active power filter," *Trans. Inst. Meas. Control*, vol. 40, no. 12, pp. 3549–3559, 2018.

[25] Z. Feng and J. Fei, "Super-twisting sliding mode control for micro gyroscope based on RBF neural network," *IEEE Access*, vol. 6, pp. 64993–65001, 2018.

[26] Y. Yin, X. Zhao, and X. Zheng, "New stability and stabilization conditions of switched systems with mode-dependent average dwell time," *Circuits Syst. Signal Process.*, vol. 36, no. 1, pp. 82–98, 2017.

[27] Y. Yin, G. Zong, and X. Zhao, "Improved stability criteria for switched positive linear systems with average dwell time switching," *J. Franklin Inst.*, vol. 354, no. 8, pp. 3472–3484, May 2017.

[28] X. Huo, L. Ma, X. Zhao, and G. Zong, "Observer-based fuzzy adaptive stabilization of uncertain switched stochastic nonlinear systems with input quantization," *J. Franklin Inst.*, vol. 356, no. 4, pp. 1789–1809, 2019.

MIN ZHANG received the B.S. degree in electrical engineering and automation from Xidian University, Xi'an, China, in 2009, the M.S. degree in control theory and engineering from the Xi'an Institute of Optics and Precision Mechanics, Chinese Academy of Sciences, Xi'an, China, in 2012, and the Ph.D. degree in mechatronics engineering from the Changchun Institute of Optics, Fine Mechanics and Physics, Chinese Academy of Sciences, Changchun, China, in 2016. Her research interests include optical communication and the field of control theory, and beaconless acquisition technology.

YUNJIE TENG received the B.S. degree from the School of Optoelectronic Engineering Technology, Changchun University of Science and Technology, Changchun, China, in 2015, where he is currently pursuing the Ph.D. degree. His research interests include optical communication and the field of control theory, and beaconless acquisition technology.

SHOUFENG TONG received the Ph.D. degree from the Department of Electronic Information, Changchun Institute of Optics, Fine Mechanics and Physics, Chinese Academy of Sciences, Jilin, China. He is currently a Professor with the Changchun University of Science and Technology. He currently specializes in optical engineering, and is the provincial Key Leader of a team responsible for teaching in that field. His current research interests are in the laser communication and telemetry remote sensing technology. He was a recipient of the Yangtze River Scholar Award, in 2014.

• • •